

## Article

# Forest Fire Detection of FY-3D Using Genetic Algorithm and Brightness Temperature Change

Zhangyu Dong <sup>1,2,3,\*</sup>, Jinqiu Yu <sup>1,3</sup>, Sen An <sup>1,3</sup>, Jin Zhang <sup>1,3</sup>, Jinhui Li <sup>1,3</sup> and Daoli Xu <sup>1,3</sup>

<sup>1</sup> School of Computer and Information, Hefei University of Technology, Hefei 230601, China; yu\_jinqiu@126.com (J.Y.); 2020111017@mail.hfut.edu.cn (S.A.); zhangjin0129@163.com (J.Z.); ljh13865256714@163.com (J.L.); xudaoli950806@163.com (D.X.)

<sup>2</sup> Intelligent Interconnected Systems Laboratory of Anhui Province, Hefei 230009, China

<sup>3</sup> Anhui Province Key Laboratory of Industry Safety and Emergency Technology, Hefei 230601, China

\* Correspondence: dzyhfut@hfut.edu.cn

**Abstract:** As one of China's new generation polar-orbiting meteorological satellites, FengYun-3D (FY-3D) provides critical data for forest fire detection. Most of the existing related methods identify fire points by comparing the spatial features and setting thresholds empirically. However, they ignore temporal features that are associated with forest fires. Besides, they are difficult to generalize to multiple areas with different environmental characteristics. A novel method based on FY-3D combining the genetic algorithm and brightness temperature change detection is proposed in this work to improve these problems. After analyzing the spatial features of the FY-3D data, it adaptively detects potential fire points based on these features using the genetic algorithm, then filters the points with contextual information. To address the false alarms resulting from the confusing spectral characteristics between fire pixels and conventional hotspots, temporal information is introduced and the "MIR change rate" based on the multitemporal brightness temperature change is further proposed. In order to evaluate the performance of the proposed algorithm, several fire events occurring in different areas are used for testing. The Moderate-Resolution Imaging Spectroradiometer (MODIS) Thermal Anomalies/Fire products (MYD14) is chosen as the validation data to assess the accuracy of the proposed algorithm. A comparison of results demonstrates that the algorithm can identify fire points effectively and obtain a higher accuracy than the previous FY-3D algorithm.

**Keywords:** fire detection; genetic algorithm; change detection; FY-3D



**Citation:** Dong, Z.; Yu, J.; An, S.; Zhang, J.; Li, J.; Xu, D. Forest Fire Detection of FY-3D Using Genetic Algorithm and Brightness Temperature Change. *Forests* **2022**, *13*, 963. <https://doi.org/10.3390/f13060963>

Academic Editors: Olga Viedma and Chunying Ren

Received: 30 March 2022

Accepted: 17 June 2022

Published: 20 June 2022

**Publisher's Note:** MDPI stays neutral with regard to jurisdictional claims in published maps and institutional affiliations.



**Copyright:** © 2022 by the authors. Licensee MDPI, Basel, Switzerland. This article is an open access article distributed under the terms and conditions of the Creative Commons Attribution (CC BY) license (<https://creativecommons.org/licenses/by/4.0/>).

## 1. Introduction

Forest fires are happening every day on the planet, which has a serious impact on human society and the ecological environment [1–4]. On average, there are more than 220,000 fires in the world every year, and the burning area exceeds 1.8% of the total global forest area [5]. Forest fires represent a major factor in soil erosion as well as air pollution, and also have a severe impact on human life safety [6–8]. Therefore, accurate identification of fire information is critical.

Forest fire detection is divided into traditional methods and remote sensing methods. Traditional methods, such as observation stations and ground patrols, have to devote a large amount of manpower, materials, and funds, and they have difficulty in detecting the dynamics of fires in time [9]. Satellite data overcome these drawbacks and have become an important source of information for fire detection [10]. Dozier [11] first used mid-infrared (MIR) and thermal-infrared (TIR) data of the Advanced Very High-Resolution Radiometer (AVHRR) for sub-pixel temperature inversion, and then Flass and Ceccato [12] proposed an algorithm for fire identification based on background information. With the successful launch of MODIS, the development of fire detection has entered a new stage. Kaufman et al. [13] used MODIS signals at 4  $\mu\text{m}$  and 11  $\mu\text{m}$  to separate the fire signal from the background signal. Giglio et al. [14] improved this and proposed an enhanced contextual

detection algorithm. This method first marks a pixel as a “potential fire point” by a series of fixed thresholds, and then determines whether the pixel is a “true fire point” based on comparisons of the candidate hot pixel with the background information. This approach has now been updated to version 6 and has generated a stable and reliable set of MODIS fire products [15].

It has been proven that the contextual algorithm of MODIS can support different types of satellite data [16–23]. Among them, polar-orbiting and geostationary satellites with rich spectral information have demonstrated excellent capabilities in disaster detection [24,25]. Due to the extremely high temporal resolution of geostationary satellites, a series of fire monitoring algorithms based on temporal variation and spatial analysis which take into account both temporal and spatial information have been developed [26–29]. However, the low spatial resolution of geostationary satellites and the omission of small fires limit their applications [29]. Compared with geostationary satellites, polar-orbiting satellites can provide good resolution. At present, researchers have also carried out studies on the temporal information of polar-orbiting satellites [30–32], but how to integrate the spatial information still needs further exploration.

The genetic algorithm (GA) is a population-based metaheuristic algorithm that utilizes multiple candidate solutions during the search process, maintaining diversity in the population and avoiding the solutions from being stuck in local optima [33]. In the field of remote sensing, GA has been proven to be effective for geological disaster mapping [34–36], but there is still a lack of research on GA in the field of fire. In this paper, we propose a fire detection method combining GA and brightness temperature change detection for China’s second-generation polar-orbiting meteorological satellite FY-3D. The existing fire detection algorithm based on FY-3D is similar to the contextual algorithm, which analyzes the MIR value in the whole scene, and selects a fixed difference threshold compared with the minimum value of MIR to extract potential fire points [23]. However, because of the temporal and spatial variability of the natural background, the fixed threshold may not be suitable for all regions. Moreover, the neglect of temporal information is a limitation of the method. To address these drawbacks, we propose to use GA to evaluate the optimal threshold of potential fire points to improve the regional adaptability of the algorithm. In addition, we used the brightness temperature change detection of the images before and after the fire to reduce the misjudgment caused by conventional hot spots. We evaluated the accuracy of the proposed algorithm with reference to MODIS fire product MYD14 and compared the results with those of the previous FY-3D algorithm.

## 2. Data Sources

Fengyun-3 meteorological satellites are China’s second-generation polar-orbiting meteorological satellites, with substantively enhanced functionalities and technical capabilities. They are designed to enhance China’s three-dimensional atmospheric sounding capability and global data acquisition capability [37]. FY-3D, as the fourth satellite, was launched on 15 November 2017. It is jointly networked with FY-3C to improve the accuracy of atmospheric detection and enhance the capabilities of greenhouse gas monitoring, comprehensive space environment detection, and meteorological remote sensing detection [38,39]. The FY-3D L1 level data used in this article can be downloaded from the National Satellite Meteorological Center (<http://satellite.nsmc.org.cn/portalsite/default.aspx> (accessed on 27 May 2022)).

Medium Resolution Spectral Imager II (MERSI-II) is one of the core instruments of FY-3D satellite and has become one of the most advanced wide-range imaging remote sensing instruments in the world after upgrading and improvement. The sensor integrates the functions of FY-3C MERSI and Visible and Infra-Red Radiometer (VIRR) sensors. The spatial resolution of its data includes 250 and 1000 m, with a total of 25 spectral channels [40]. According to the Wien displacement law [41], the proposed algorithm in this paper primarily uses the MIR channel 20 and TIR channel 24 to detect fires, and the visible channels 12 and 15 to eliminate clouds and sun glint in the atmospheric profile. The

information on the spectral and spatial characteristics of the MERSI-II channels used in the algorithm is given in Table 1.

**Table 1.** Spectral characteristics of FY-3D MERSI.

Channel	Center Wavelength ( $\mu\text{m}$ )	Spectral Bandwidth (nm)	SNR or NE $\Delta$ T (K)	Resolution (m)
1	0.47	50	100	250
2	0.55	50	100	250
3	0.65	50	100	250
12	0.67	20	500	1000
15	0.865	20	500	1000
20	3.8	180	0.25 K	1000
24	10.8	1000	0.4 K	250
25	12.0	1000	0.4 K	250

### 3. Method

The logical structure of the algorithm in this paper is shown in Figure 1. As the flowchart indicates, the proposed algorithm has four steps. The first step is data preprocessing, which consists of radiometric calibration and geometric correction. The second step is fire monitoring. This step inherits the enhanced contextual algorithm of MODIS, but we use GA to extract potential fire points to improve the automatic adaptability of the algorithm. The third step is to eliminate misjudgment and filter out some non-fire pixels whose spectral features are similar to fire points. The final step is the validation of the results. We choose the MODIS active fire products MYD14 as the reference data and compare the detection results with those obtained using the previous FY-3D algorithm to assess the performance of the proposed algorithm.

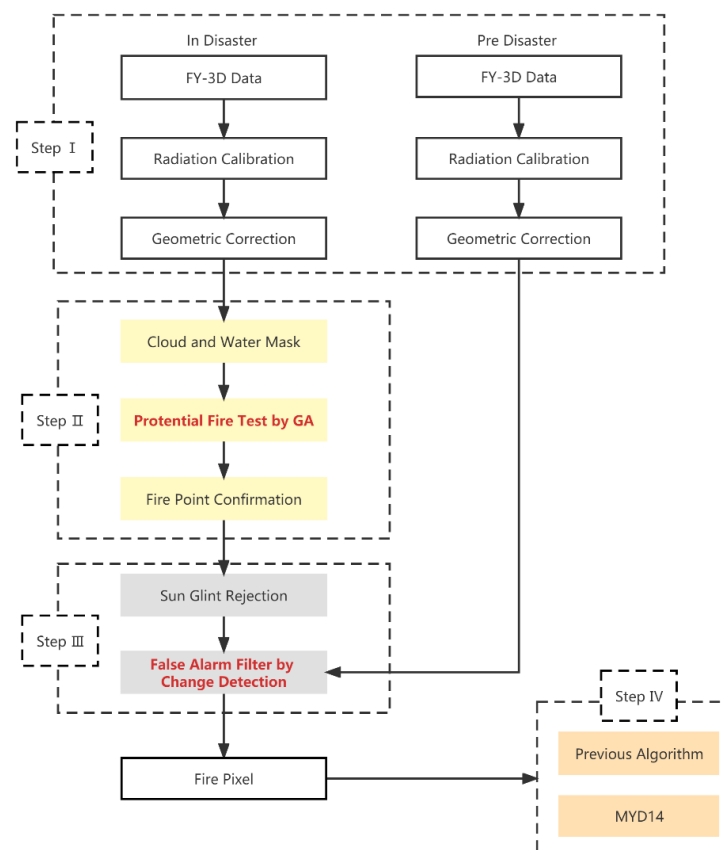


**Figure 1.** Flowchart of the proposed detection algorithm in this paper.

### 3.1. Cloud and Water Masking

Cloud and water pixels should be excluded before fire detection. The 12, 15, and 25 channels of MERSI data are used for cloud removal. A cell is defined as a cloud if it meets a combination of the following conditions

Daytime:

$$\begin{aligned} & (r_{12} + r_{15} > 1.2) \text{ or } (T_{25} < 265 \text{ K}) \text{ or} \\ & (r_{12} + r_{15} > 0.7 \text{ and } T_{25} < 285 \text{ K}) \text{ or} \\ & (\text{water pixel and } r_{15} > 0.25 \text{ and } T_{25} < 300 \text{ K}) \end{aligned} \quad (1)$$

Nighttime:

$$T_{25} < 265 \text{ K} \quad (2)$$

The reflectance and the brightness temperature with channel  $i$  are denoted as  $r_i$  and  $T_i$ , and water pixels are automatically identified using the "Land and Sea Mask" dataset provided in the MERSI L1 files. After this step, cloud and water pixels will be excluded from effective background pixels and will not be used in the subsequent calculation.

### 3.2. Potential Fire Identification

This process is used to remove obvious non-fire pixels. However, due to the different environments of each area, the optimal threshold of potential fire points is also different. Therefore, we choose the genetic algorithm to extract potential fire points automatically and adaptively.

The genetic algorithm was first proposed by Professor Holland of the United States in his monograph on the adaptability of nature and artificial systems in 1975 [42]. It is a kind of random search algorithm based on natural selection and natural genetic mechanisms in the biological world. In this section, the genetic algorithm is used to segment the image by maximizing the inter-class variance and minimizing the intra-class variance [43]. The main process is as follows.

Population initialization is the first step. An individual is equal to a chromosome, and each chromosome corresponds to a threshold solution to the problem. Each threshold is defined as a binary bit vector of length  $L$ , and each binary bit is called a gene. In this paper, the brightness temperature value of channel 20 is selected as the pixel value, and the saturation value of this channel is 350 K. Therefore, the gene length  $L$  of each chromosome is defined as 9.

The second step is an adaptive assessment and ranking. Otsu is selected as the fitness function here. For different thresholds, the greater the inter-class variance and the smaller the intra-class variance, the better the segmentation effect [44]:

$$F(\text{fitness}, t) = \omega_1 \times \omega_2 \times (m_0 - m_1)^2 \quad (3)$$

where  $m_0$ ,  $m_1$  are the mean of background pixels and object pixels in the segment whose threshold value is  $t$ , and these parameters are given as:

$$\omega_0 = \sum_{i=1}^t P_i \quad (4)$$

$$\omega_1 = 1 - \omega_0 \quad (5)$$

$$m_0 = \frac{\sum_{i=1}^t iP_i}{\omega_0} \quad (6)$$

$$m_1 = \frac{\sum_{i=1}^{2^L} iP_i}{\omega_1} \quad (7)$$

The next step is to select chromosomes to create a new population. In this paper, by using roller wheel, each chromosome is allocated to the roulette with a probability of 1 according to the proportion of fitness, then the random numbers between 0 and 1 are generated and the chromosomes corresponding to the random numbers are selected

according to the cumulative probability distribution. This approach makes it easier for chromosomes with high fitness to be selected.

After that, the selected chromosomes are crossed and mutated, then is repeated from the second step until the number of iterations is reached, and the threshold solution with the highest fitness is output.

Therefore, the potential fire point needs to meet the following requirements:

$$T_{20} > t \quad (8)$$

$$\Delta T > [\overline{\Delta T}, 8]_{\min} \quad (9)$$

where  $t$  is the threshold obtained by genetic algorithm, and  $\overline{\Delta T}$  is the mean value of  $\Delta T$  ( $\Delta T = T_{20} - T_{24}$ ) after removing cloud and water pixels.

### 3.3. Fire Point Confirmation

#### 3.3.1. Absolute Threshold Test

Referring to the algorithm proposed by Giglio et al. [14] and considering the saturation temperature of the MERSI channel, the absolute threshold detection is as follows:

$$T_{20} > 350 \text{ K} (320 \text{ K at night}) \quad (10)$$

The potential fire pixels that pass the test are marked as fire points, and the remaining will be further tested.

#### 3.3.2. Contextual Test

Contextual detection has a better effect on small and low-temperature fires. The test makes full use of the background information to judge the potential fire pixel according to the difference between the pixel to be detected and its surrounding pixels. First, a scanning window is created centered on the potential fire pixel. In this window, pixels that satisfy the following, (1) are not cloud-contaminated or water-contaminated, (2) are not background fire pixels (those potential fire pixels generated using the genetic algorithm described in Section 3.2), are defined as valid. The window starts with a  $3 \times 3$  pixels square ring and increases to a maximum of  $21 \times 21$  pixels until at least 25% of the pixels within the window are valid and the number of valid pixels is at least eight. Otherwise, the detection pixel will be classified as a non-fire point [14]. After the background characterization is successful, a series of contextual threshold tests will be performed for relative fire detection:

$$\Delta T > \overline{\Delta T} + 3.5 \times \delta_{\Delta T} \quad (11)$$

$$\Delta T > \overline{\Delta T} + 6 \quad (12)$$

$$T_{20} > \overline{T_{20}} + 4 \times \delta_{T_{20}} \quad (13)$$

$$T_{24} > \overline{T_{24}} + \delta_{T_{24}} - 4 \quad (14)$$

$$\delta'_{T_{20}} > 5 \quad (15)$$

where  $\overline{\Delta T}$  and  $\delta_{\Delta T}$  are the mean and mean absolute deviation of  $\Delta T$  for the valid pixels,  $\overline{T_{20}}$  and  $\delta_{T_{20}}$  are the mean and mean absolute deviation of  $T_{20}$  for the valid pixels,  $\overline{T_{24}}$  and  $\delta_{T_{24}}$  are the mean and mean absolute deviation of  $T_{24}$  for the valid pixels, and  $\delta'_{T_{20}}$  is the mean absolute deviation of  $T_{20}$  for the background fire pixels.

A daytime pixel is tentatively classified as a fire pixel if it not only satisfies (11)–(13), but also one of (14) and (15), while a nighttime pixel only needs to satisfy (11)–(13).

### 3.4. Sun Glint Rejection

The water and land boundaries and cirrus cloud boundaries in remote sensing images sometimes reflect sunlight back due to the observation angle of satellite sensors, resulting

in abnormal brightness temperatures in the MIR band and forming false fires. In order to improve the accuracy of fire recognition, it is necessary to detect sun glints and eliminate them. Here,  $\theta_g$  is the angle between vectors pointing in the surface-to-satellite and specular reflection directions:

$$\cos \theta_g = \cos \theta_v \cos \theta_s - \sin \theta_v \sin \theta_s \cos \phi \quad (16)$$

where  $\theta_v$  and  $\theta_s$  are the view and solar zenith angles, respectively, and  $\phi$  is the relative azimuth angle. The following conditions are then evaluated:

$$(\theta_g < 10^\circ \text{ and } r_{12} + r_{15} > 0.2) \quad (17)$$

If condition (17) is satisfied, the fire pixel is rejected as sun glint and classified as non-fire.

### 3.5. False Alarms Filter

In this paper, change detection is used for false alarm filtering. We use the previous image without fire to compare with the detection image to determine if a fire pixel has changed. If not, the fire pixel is excluded as a non-fire pixel. This process effectively eliminates conventional hot-spots that have been misclassified as fires.

The change detection proposed by Parto et al. [45] sets the threshold dynamically based on the difference of the average temperature of the MIR channel between the two images. Considering that there may be outliers in remote sensing images, this paper does not choose the average value but the median for change detection, because the median is not affected by the extreme value, but also reflects the intermediate level.

We chose the MIR channel for change detection and calculated the “MIR change rate”, namely  $R$ . In the relevant parameters,  $T_d$  is the brightness temperature of the 20 channel of the detection image,  $T_p$  is the brightness temperature of the 20 channel of the previous image. The median  $T_d$  and median  $T_p$  for the pixels are computed and denoted as  $M_d$  and  $M_p$ :

$$R = \frac{T_d - T_p}{|M_d - M_p|} \quad (18)$$

We chose two different types of pixels for comparative analysis, namely fire and non-fire, where the fire was generated by MYD14. Figure 2 shows the box-plot of  $R$ -value. We can see that  $R$  has a good separation ability, and the value of fire point is significantly higher than that of non-fire point, demonstrating that filtering the false alarm with  $R$  is reasonable.

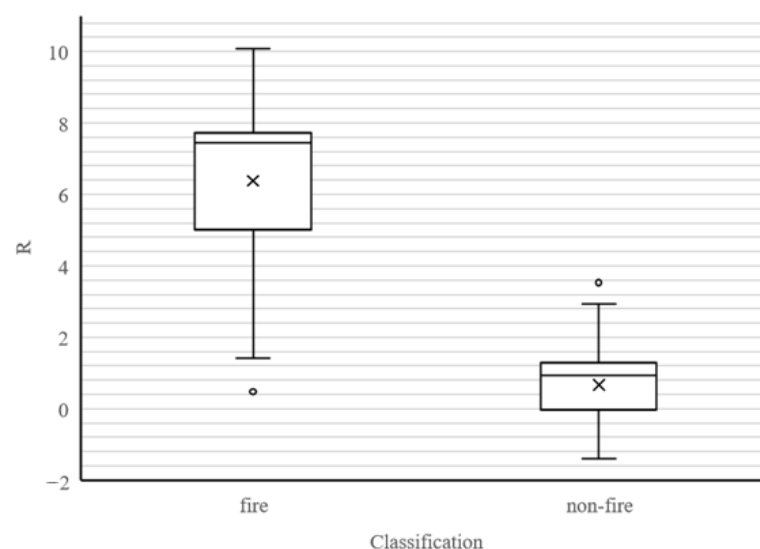


Figure 2. Box-plot of  $R$ .

From Figure 2, we can see that the R of fire points is mainly above 1.5, but there are also a few outliers with an R-value below 1.5. As commonly known, there is an opposite relationship between commission error and omission error, but in order to minimize omissions as much as possible, we choose 1.5 as the detection threshold of R, that is:

$$R > 1.5 \quad (19)$$

The fire pixel satisfying condition (19) remains unchanged. On the contrary, it is determined as a misjudgment of fire point, which is classified as a non-fire point.

#### 4. Results and Discussion

To test the performance of the algorithm, several fire events with a worldwide distribution that occurred in the past three years were selected. The validation work carried out in this study aims to test the accuracy of the proposed algorithm and to demonstrate its superiority over the previous FY-3D algorithm. Due to the difficulty in obtaining ground truth fire data, researchers usually use remote sensing data for validation. The MODIS active fire products have been used in various scientific studies and practical operations over the last decade and are recognized as stable data. Therefore, for this validation exercise, we have chosen to use the MODIS active fire product MYD14 and the results obtained by the previous FY-3D algorithm to meet the validation goals. All parameters of the previous algorithm were set according to the method of the original paper. MYD14 can be downloaded from Level-1 and Atmosphere Archive & Distribution System Distributed Active Archive Center (<https://ladsweb.modaps.eosdis.nasa.gov/> (accessed on 27 May 2022)). Detailed information on accuracy and error rates is shown in Table 2. Because of the differences between the MODIS and FY-3D MERSI-II, we introduced a 1-pixel buffer in the calculation of the accuracy and error rates.

**Table 2.** Detailed statistical results of each fire detection algorithm compared with MYD14.

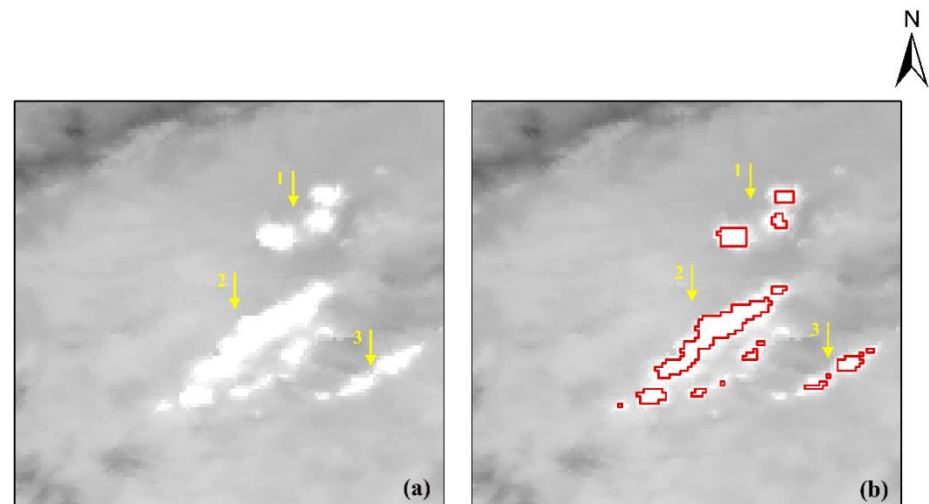
Area	Imaging Data	Accuracy		Commission Error		Omission Error	
		Current	Previous	Current	Previous	Current	Previous
Khabarovsk	2019/4/16	71.09%	70.39%	28.91%	29.06%	5.91%	4.93%
Siberia	2019/8/5	84.68%	76.18%	15.31%	23.81%	20.10%	7.73%
Amazon	2019/8/23	84.12%	70.98%	15.87%	29.01%	17.85%	9.52%
California	2019/10/28	83.33%	80.55%	16.67%	19.44%	7.69%	7.89%
Western Australia	2020/1/1	93.55%	71.74%	6.45%	28.26%	6.66%	6.67%
Sichuan	2020/3/30	67.65%	47.72%	32.35%	52.28%	7.92%	3.65%
Bodrum	2021/8/5	83.54%	65.88%	16.45%	34.11%	14.03%	19.29%

Note: Accuracy indicates the true detection rates of MERSI fire pixels. A MERSI fire pixel within the 1-pixel buffer of MYD14 was considered as truly detected, otherwise it was considered as a commission error. Omission errors were defined as MYD14 fire pixels with no coincident pixel in 1-pixel buffer of MERSI fire pixel.

As shown in Table 2, the accuracy of the proposed algorithm exceeds 80% in most examples. Figures 3 and 4 show the results of the proposed algorithm in Khabarovsk, Russia, and Bodrum, Turkey. Figures 3a and 4a show the MIR channel images of the detected areas. The yellow arrows in the figures point to the location of the fire areas. As can be seen from Figures 3b and 4b, the proposed algorithm can detect the location of the fire accurately.

By comparing the results of the proposed algorithm and the previous algorithm in Table 2, we found that the accuracy of the proposed algorithm is significantly higher than that of the previous algorithm. The previous algorithm was less adaptable to different regions and had a large variation in detection performance. The proposed algorithm has been improved in this aspect. However, omission error is also an important indicator of evaluation. We found that the omission errors are still relatively serious, even up to 20% in the Amazon and Russia. The main reason for omission errors is the step where the genetic algorithm extracts potential fire points. Our approach of maximizing inter-class variance

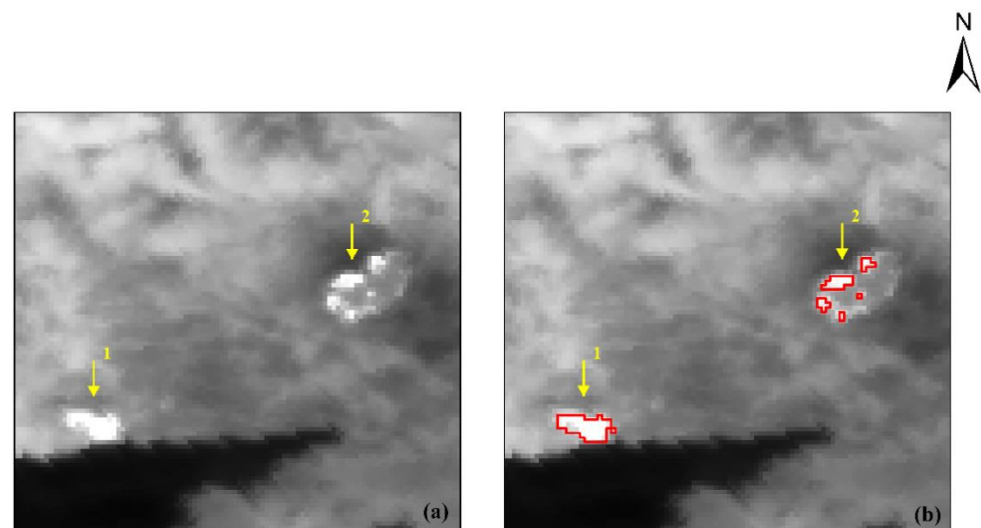
and minimizing intra-class variance to assess the fitness of different solutions led to a high threshold and filtering out some small and low-temperature fire points. In addition, the detection results of the proposed algorithm were close to those of the previous algorithms in some areas, such as California and Khabarovsk. This may be because the two methods in these regions have close thresholds in potential fire point extraction, and the fixed threshold of brightness temperature change detection in false alarm filtering is low and may have difficulty working for some areas. Overall, although this method has some problems, it is improved in many aspects compared with the previous algorithm, providing a new choice for fire detection based on FY-3D.



#### Fire detection

 Proposed algorithm

**Figure 3.** Fire detection results in Khabarovsk, Russia, on 16 April 2019. (a) MIR channel image; (b) Detection results of the proposed algorithm.



#### Fire detection

 Proposed algorithm

**Figure 4.** Fire detection results in Bodrum, Turkey, on 5 August 2021. (a) MIR channel image; (b) Detection results of the proposed algorithm.

#### 4.1. Comparison with MYD14

MODIS Fire and Thermal Anomaly products are globally recognized as products with strong stability. This paper also uses the product MYD14 for comparison to prove the effectiveness of the proposed algorithm.

Figures 5 and 6 are two examples. The background is composed of 3, 2 and 1 channel images at 250 m resolution of MERSI. Figure 5 shows fires in Australia on 1 January 2020. The fire locations found by this method are in good agreement with those obtained by MYD14. Figure 6 shows fires in the Amazon on 23 August 2019; it can be seen that although most fire points are detected, some small fire points are missing.

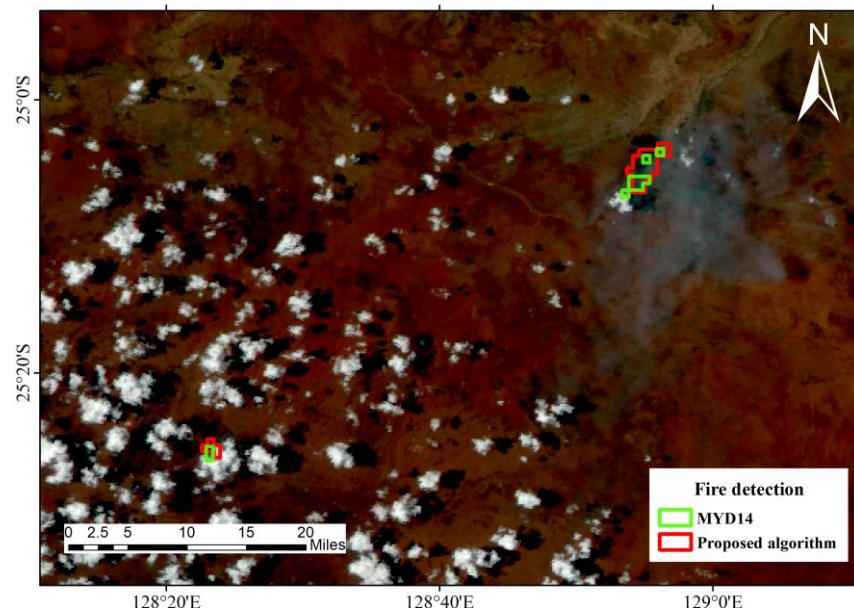


**Figure 5.** Comparison with MYD14 of 1 January 2020 fire results in Western, Australia.

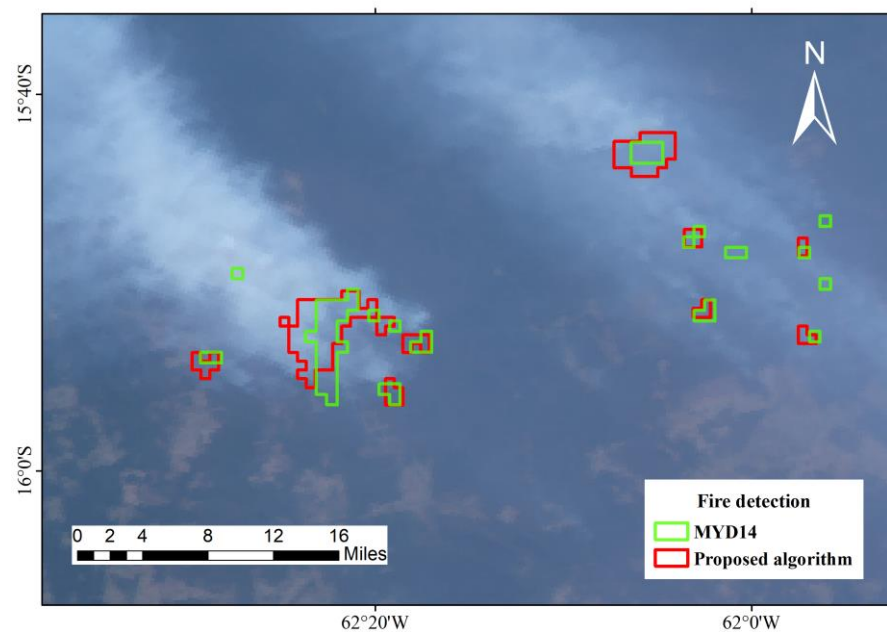


**Figure 6.** Comparison with MYD14 of 23 August 2019 fire results in the Amazon.

After analysis, we found that the overlapping position of the two results was basically in the center of the fire. The sensor and imaging time difference between MERSI and MODIS leads to a slight deviation in the location of the detected fire, which is the main

reason for the error at edges. In addition, there are some small fires covered with thick smoke, resulting in a decrease in the energy radiated to the satellite sensor, and causing low temperature omission [46]. In general, the algorithm in this paper produces comparable results to those obtained using MYD14, proving its effectiveness and stability.

#### 4.2. Comparison with Previous Algorithm

The previous FY-3D algorithm has produced good results, however there is still room for improvement in terms of accuracy. Figures 7 and 8 show the advantages of the new algorithm. It is not difficult to see that previous algorithms reduce omission errors at the expense of accuracy. Figure 7 shows the fire event in Siberia, Russia on 5 August 2019. The edge error of the previous algorithm, whose detection area is significantly larger than that of the proposed algorithm and MYD14, is obvious. However, the problem of omission in this area is slightly more serious for the proposed algorithm. Figure 8 shows the fire event in Sichuan, China on 30 March 2020. In addition to edge errors, the previous algorithm has two false detections due to the influence of smoke and the pixels with similar spectral characteristics to the fire points, which are marked in the picture. However, in this area, the results of both algorithms are worse. This is related to the difference in imaging time between MODIS and MERSI. The imaging time difference between the two sensors in this area is larger than the others and the fire has shown a tendency to spread in all directions, so the accuracy obtained by FY-3D algorithms is lower.

In summary, compared with the previous algorithm, the proposed algorithm presents a major improvement in detection accuracy and adaptability and more effectively rejects the misjudgment caused by smoke and conventional hot spots. However, there is no significant improvement in omission error, and in some areas, it is even slightly worse than before, such as Siberia, as shown in Figure 7. This indicates that the proposed algorithm can more easily miss the low-temperature fire points. In potential fire identification, the genetic algorithm suffers from the problem of setting a high threshold in the pursuit of accuracy, which is a major drawback of the proposed method.

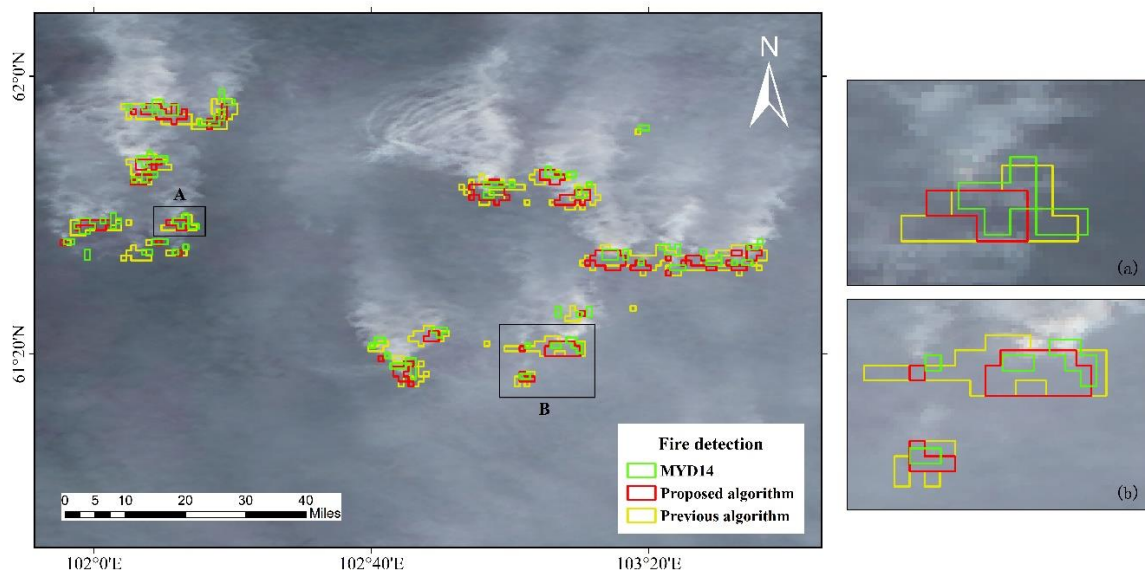


**Figure 7.** Comparison with previous algorithm of 5 August 2019 fire results in Siberia, Russia. On the right (a,b) are partial enlargements of regions A and B on the left, respectively.

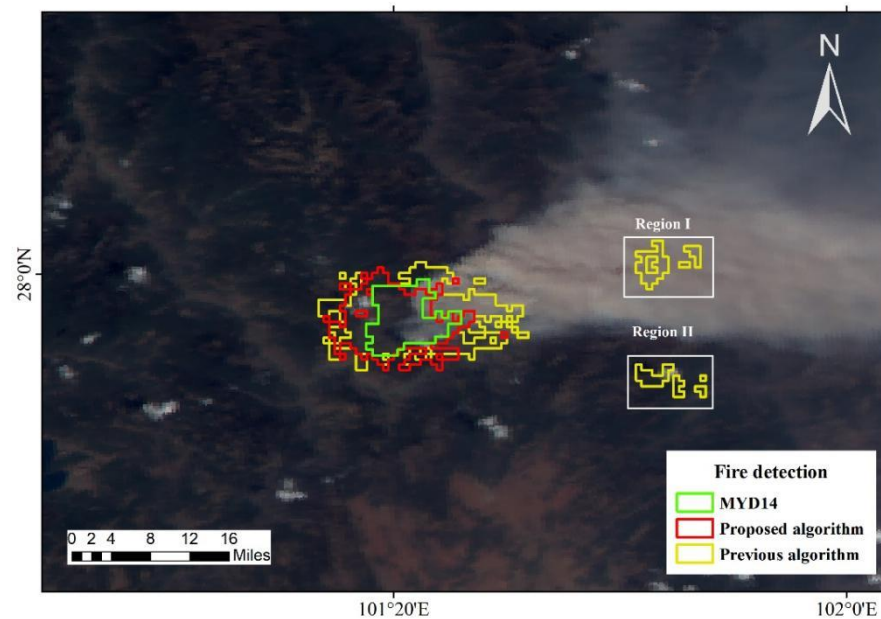


**Figure 8.** Comparison with previous algorithm of 30 March 2020 fire results in Sichuan, China.

## 5. Conclusions

FY-3D is a second-generation Chinese polar-orbiting satellite, and MERSI-II is one of the advanced sensors it carries. The current fire detection algorithm based on FY-3D MERSI-II data is similar to the enhanced contextual algorithm, and the neglect of temporal information and poor adaptivity due to fixed thresholds are the drawbacks. In order to improve the existing algorithm, we propose a fire point monitoring algorithm combining the genetic algorithm and brightness temperature change detection. The genetic algorithm is introduced to extract potential fire points to improve the regional adaptiveness, and Otsu is chosen as the fitness function of the genetic algorithm to calculate the optimal MIR threshold. Temporal information is also introduced to filter out misclassifications due to conventional hotspots with similar spectral characteristics to the fire point. To evaluate the performance of the proposed algorithm, fire events from different regions were selected for validation and compared with the previous results of the FY-3D algorithm in this paper. The results show that the accuracy of the proposed algorithm is generally above 80%, while the accuracy of the previous algorithm is above 70%. The comparison results show that the proposed algorithm performs better.

However, omission errors are still a major problem in this paper. We found that the omission was around 10% in most areas, even reaching 20% in Russia. The genetic algorithm tends to filter out small, low-temperature fires covered by dense smoke when extracting potential fires, which is a major problem of the proposed algorithm. The current infrared signals based on optical satellites are easily affected by clouds and smoke, and synthetic aperture radar (SAR) data can be considered. SAR has a certain degree of surface penetration and can be considered to complement the information from optical satellites. At the same time, fire radiated power (FRP) can help quantify the scale of fire events and should be taken into account in subsequent studies.

In addition, the “MIR change rate” presented in this paper is calculated using two images before and after the fire. If the time between images is too long, seasonal differences may affect the results. In the future, the introduction of multiple time series can be considered for detection. We also used a fixed threshold to filter false fire points for the “MIR change rate”, which does not take into account the differences between regions. This threshold could be improved to allow for automatic adaptation to different regions.

**Author Contributions:** Conceptualization, Z.D. and J.Y.; methodology, Z.D.; software, J.Y., S.A. and J.Z.; formal analysis, Z.D.; investigation, J.L. and D.X.; writing—original draft preparation, Z.D. and

J.Y.; writing—review and editing, S.A., J.Z., J.L. and D.X. All authors have read and agreed to the published version of the manuscript.

**Funding:** This research was funded by Anhui Province Key R&D Program of China (202004a07020030), and Fundamental Research Funds for the Central Universities (JZ2021HGTB0111), and Anhui Province Natural Science Foundation (2108085MF233).

**Institutional Review Board Statement:** Not applicable.

**Informed Consent Statement:** Not applicable.

**Data Availability Statement:** Data are available on request from the corresponding author.

**Conflicts of Interest:** The authors declare no conflict of interest.

## References

1. Reid, C.E.; Brauer, M.; Johnston, F.H.; Jerrett, M.; Balmes, J.R.; Elliott, C.T. Critical review of health impacts of wildfire smoke exposure. *Environ. Health Perspect.* **2016**, *124*, 1334–1343. [[CrossRef](#)] [[PubMed](#)]
2. Moritz, M.A.; Parisien, M.-A.; Batllori, E.; Krawchuk, M.A.; Van Dorn, J.; Ganz, D.J.; Hayhoe, K. Climate change and disruptions to global fire activity. *Ecosphere* **2012**, *3*, 1–22. [[CrossRef](#)]
3. Brando, P.M.; Balch, J.K.; Nepstad, D.C.; Morton, D.C.; Putz, F.E.; Coe, M.T.; Silvério, D.; Macedo, M.N.; Davidson, E.A.; Nóbrega, C.C.; et al. Abrupt increases in Amazonian tree mortality due to drought–fire interactions. *Proc. Natl. Acad. Sci. USA* **2014**, *111*, 6347–6352. [[CrossRef](#)] [[PubMed](#)]
4. Allen, C.D.; Macalady, A.K.; Chenchouni, H.; Bachelet, D.; McDowell, N.; Vennetier, M.; Kitzberger, T.; Rigling, A.; Breshears, D.D.; Hogg, E.H.; et al. A global overview of drought and heat-induced tree mortality reveals emerging climate change risks for forests. *For. Ecol. Manag.* **2010**, *259*, 660–684. [[CrossRef](#)]
5. Wu, M.-Y.; Han, N.; Luo, Q.-J. A smoke detection algorithm based on discrete wavelet transform and correlation analysis. In Proceedings of the 2012 Fourth International Conference on Multimedia Information Networking and Security, Nanjing, China, 2–4 November 2012; pp. 281–284.
6. Certini, G. Effects of fire on properties of forest soils: A review. *Oecologia* **2005**, *143*, 1–10. [[CrossRef](#)]
7. Fan, Q.; Wang, C.; Zhang, D.; Zang, S. Environmental influences on forest fire regime in the Greater Hinggan Mountains, Northeast China. *Forests* **2017**, *8*, 372. [[CrossRef](#)]
8. Johnson, D.W.; Walker, R.F.; McNulty, M.; Rau, B.M.; Miller, W.W.; Johnson, B.G. The long-term effects of wildfire and post-fire vegetation on Sierra Nevada Forest soils. *Forests* **2013**, *4*, 517. [[CrossRef](#)]
9. Tian, X.R.; Mcrae, D.J.; Shu, L.F.; Wang, M.Y.; Hong, L. Satellite remote-sensing technologies used in forest fire management. *J. For. Res.* **2005**, *16*, 7.
10. Engel, C.B.; Jones, S.D.; Reinke, K. A Seasonal-window ensemble-based thresholding technique used to detect active fires in geostationary remotely sensed data. *IEEE Trans. Geosci. Remote Sens.* **2021**, *59*, 4947–4956. [[CrossRef](#)]
11. Dozier, J. A method for satellite identification of surface temperature fields of subpixel resolution. *Remote Sens. Environ.* **1981**, *11*, 221–229. [[CrossRef](#)]
12. Flasse, S.P.; Ceccato, P. A contextual algorithm for AVHRR fire detection. *Int. J. Remote Sens.* **1996**, *17*, 419–424. [[CrossRef](#)]
13. Kaufman, Y.J.; Justice, C.O.; Flynn, L.P.; Kendall, J.D.; Prins, E.M.; Giglio, L.; Ward, D.E.; Menzel, W.P.; Setzer, A.W. Potential global fire monitoring from EOS-MODIS. *J. Geophys. Res. Atmos.* **1998**, *103*, 32215–32238. [[CrossRef](#)]
14. Giglio, L.; Descloitres, J.; Justice, C.O.; Kaufman, Y.J. An Enhanced contextual fire detection algorithm for MODIS. *Remote Sens. Environ.* **2003**, *87*, 273–282. [[CrossRef](#)]
15. Giglio, L.; Schroeder, W.; Justice, C.O. The collection 6 MODIS active fire detection algorithm and fire products. *Remote Sens. Environ.* **2016**, *178*, 31–41. [[CrossRef](#)] [[PubMed](#)]
16. Roberts, G.J.; Wooster, M.J. Fire detection and fire characterization over Africa using Meteosat SEVIRI. *IEEE Trans. Geosci. Remote Sens.* **2008**, *46*, 1200–1218. [[CrossRef](#)]
17. Wooster, M.; Xu, W.; Nightingale, T. Sentinel-3 SLSTR active fire detection and FRP product: Pre-launch algorithm development and performance evaluation using MODIS and ASTER datasets. *Remote Sens. Environ.* **2012**, *120*, 236–254. [[CrossRef](#)]
18. Schroeder, W.; Oliva, P.; Giglio, L.; Csiszar, I.A. The New VIIRS 375 m active fire detection data product: Algorithm description and initial assessment. *Remote Sens. Environ.* **2014**, *143*, 85–96. [[CrossRef](#)]
19. Csiszar, I.; Schroeder, W.; Giglio, L.; Ellicott, E.; Vadrevu, K.P.; Justice, C.O.; Wind, B. Active fires from the Suomi NPP visible infrared imaging radiometer suite: Product status and first evaluation results. *J. Geophys. Res. Atmos.* **2014**, *119*, 803–816. [[CrossRef](#)]
20. Schroeder, W.; Oliva, P.; Giglio, L.; Quayle, B.; Lorenz, E.; Morelli, F. Active fire detection using Landsat-8/OLI data. *Remote Sens. Environ.* **2016**, *185*, 210–220. [[CrossRef](#)]
21. Xu, G.; Zhong, X. Real-time wildfire detection and tracking in Australia using geostationary satellite: Himawari-8. *Remote Sens. Lett.* **2017**, *8*, 1052–1061. [[CrossRef](#)]

22. Lin, Z.; Chen, F.; Li, B.; Yu, B.; Shirazi, Z.; Wu, Q.; Wu, W. FengYun-3C VIRR active fire monitoring: Algorithm description and initial assessment using MODIS and Landsat data. *IEEE Trans. Geosci. Remote Sens.* **2017**, *55*, 6420–6430. [[CrossRef](#)]
23. Yin, Z.; Chen, F.; Lin, Z.; Yang, A.; Li, B. Active fire monitoring based on FY-3D MERSI satellite data. *Remote Sens. Technol. Appl.* **2020**, *35*, 1099–1108. [[CrossRef](#)]
24. Barmpoutis, P.; Papaioannou, P.; Dimitropoulos, K.; Grammalidis, N. A review on early forest fire detection systems using optical remote sensing. *Sensors* **2020**, *20*, 6442. [[CrossRef](#)] [[PubMed](#)]
25. Szpakowski, D.M.; Jensen, J.L.R. A review of the applications of remote sensing in fire ecology. *Remote Sens.* **2019**, *11*, 2638. [[CrossRef](#)]
26. Roberts, G.; Wooster, M.J. Development of a multi-temporal Kalman filter approach to geostationary active fire detection & fire radiative power (FRP) estimation. *Remote Sens. Environ.* **2014**, *152*, 392–412. [[CrossRef](#)]
27. Xie, Z.; Song, W.; Ba, R.; Li, X.; Xia, L. A spatiotemporal contextual model for forest fire detection using Himawari-8 satellite data. *Remote Sens.* **2018**, *10*, 1992. [[CrossRef](#)]
28. Hally, B.; Wallace, L.; Reinke, K.; Jones, S.; Skidmore, A. Advances in active fire detection using a multi-temporal method for next-generation geostationary satellite data. *Int. J. Digit. Earth* **2018**, *12*, 1030–1045. [[CrossRef](#)]
29. Lin, Z.; Chen, F.; Li, B.; Yu, B.; Jia, H.; Zhang, M.; Liang, D. A contextual and multitemporal active-fire detection algorithm based on FengYun-2G S-VISSR data. *IEEE Trans. Geosci. Remote Sens.* **2019**, *57*, 8840–8852. [[CrossRef](#)]
30. Kushida, K. Detection of active wildland fires using multitemporal MODIS images. *IEEE Geosci. Remote Sens. Lett.* **2010**, *7*, 301–305. [[CrossRef](#)]
31. Panuju, D.; Trisasonjko, B.; Susetyo, B.; Raimadoya, M.; Lees, B. Historical fire detection of tropical forest from NDVI time-series data: Case study on Jambi, Indonesia. *ITB J. Sci.* **2010**, *42*, 49–66. [[CrossRef](#)]
32. Lin, Z.; Chen, F.; Niu, Z.; Li, B.; Yu, B.; Jia, H.; Zhang, M. An active fire detection algorithm based on multi-temporal FengYun-3C VIRR data. *Remote Sens. Environ.* **2018**, *211*, 376–387. [[CrossRef](#)]
33. Katoch, S.; Chauhan, S.S.; Kumar, V. A review on genetic algorithm: Past, present, and future. *Multimed. Tools Appl.* **2021**, *80*, 8091–8126. [[CrossRef](#)] [[PubMed](#)]
34. Chen, Y.-R.; Chen, J.-W.; Hsieh, S.-C.; Ni, P.-N. The application of remote sensing technology to the interpretation of land use for rainfall-induced landslides based on genetic algorithms and artificial neural networks. *IEEE J. Sel. Top. Appl. Earth Obs. Remote Sens.* **2009**, *2*, 87–95. [[CrossRef](#)]
35. Dou, J.; Chang, K.-T.; Chen, S.; Yunus, A.P.; Liu, J.-K.; Xia, H.; Zhu, Z. Automatic case-based reasoning approach for landslide detection: Integration of object-oriented image analysis and a genetic algorithm. *Remote Sens.* **2015**, *7*, 4318–4342. [[CrossRef](#)]
36. Saleh, A.; Yuzir, A.; Sabtu, N.; Abujayyab, S.K.M.; Bunmi, M.R.; Pham, Q.B. Flash flood susceptibility mapping in urban area using genetic algorithm and ensemble method. *Geocarto Int.* **2022**, *1*–30. [[CrossRef](#)]
37. Yang, A.; Zhong, B.; Wu, S.; Liu, Q. Evaluation on radiometric capability of Chinese optical satellite sensors. *Sensors* **2017**, *17*, 204. [[CrossRef](#)]
38. Yang, Z.; Zhang, P.; Gu, S.; Hu, X.; Tang, S.; Yang, L.; Xu, N.; Zhen, Z.; Wang, L.; Wu, Q.; et al. Capability of Fengyun-3D satellite in Earth system observation. *J. Meteorol. Res.* **2019**, *33*, 1113–1130. [[CrossRef](#)]
39. Zou, X. Studies of FY-3 Observations over the past 10 years: A review. *Remote Sens.* **2021**, *13*, 673. [[CrossRef](#)]
40. Wang, H.; Mao, K.; Mu, F.; Shi, J.; Yang, J.; Li, Z.; Qin, Z. A split window algorithm for retrieving land surface temperature from FY-3D MERSI-2 data. *Remote Sens.* **2019**, *11*, 2083. [[CrossRef](#)]
41. Boyer, T.H. Thermodynamics of the harmonic oscillator: Wien's displacement law and the Planck spectrum. *Am. J. Phys.* **2003**, *71*, 866–870. [[CrossRef](#)]
42. Holland, J. *Adaptation in Natural and Artificial Systems*; University of Michigan Press: Ann Arbor, MI, USA, 1975.
43. Banimelhem, O.; Yahya, Y.A. Multi-thresholding image segmentation using genetic algorithm. In Proceedings of the International Conference on Image Processing, Computer Vision, & Pattern Recognition (IPCV), Las Vegas, NV, USA, 18 July–21 July 2011.
44. Wang, C.; Wang, S.; Zhang, C.; Zou, J. Maximum variance image segmentation based on improved genetic algorithm. In Proceedings of the Eighth ACIS International Conference on Software Engineering, Artificial Intelligence, Networking, and Parallel/Distributed Computing (SNPD 2007), Qingdao, China, 30 July–1 August 2007; Volume 2, pp. 491–494.
45. Parto, F.; Saradjian, M.; Homayouni, S. MODIS brightness temperature change-based forest fire monitoring. *J. Indian Soc. Remote Sens.* **2020**, *48*, 163–169. [[CrossRef](#)]
46. Liu, S.; Li, X.; Qin, X.; Sun, G.; Liu, Q. Adaptive threshold method for active fire identification based on GF-4 PMI data. *J. Remote Sens.* **2020**, *24*, 215–225. [[CrossRef](#)]